

# Imaged sub-stellar companions: not as eccentric as they appear? The effect of an unseen inner mass on derived orbits

Tim D. Pearce<sup>\*</sup>, Mark C. Wyatt and Grant M. Kennedy

*Institute of Astronomy, University of Cambridge, Madingley Road, Cambridge, CB3 0HA, UK*

Released 2002 Xxxxx XX

## ABSTRACT

Increasing numbers of sub-stellar companions are now being discovered via direct imaging. Orbital elements for some of these objects have been derived using star-companion astrometry, and several of these appear to have eccentricities significantly greater than zero. We show that stellar motion caused by an undetected inner body may result in the companion elements derived in such a way being incorrect, which could lead to an overestimation of the eccentricity. The magnitude of this effect is quantified in several regimes and we derive the maximum eccentricity error a third body could introduce in a general form, which may be easily applied to any imaged system. Criteria for identifying systems potentially susceptible to this scenario are presented, and we find that around half of the planets/companion brown dwarfs currently imaged could be liable to these errors when their orbital elements are derived. In particular, this effect could be relevant for systems within 100 pc with companions at  $>50$  AU, if they also harbour an unseen  $\sim 10$  Jupiter mass object at  $>10$  AU. We use the Fomalhaut system as an example and show that a 10% error could be induced on the planet's eccentricity by an observationally allowed inner mass, which is similar in size to the current error from astrometry.

**Key words:** Astrometry and celestial mechanics: astrometry – Planetary Systems: planets and satellites: general – Stars: individual: Fomalhaut

## 1 INTRODUCTION

The past two decades have witnessed the birth of direct imaging as a technique to detect sub-stellar companions, with the first discovery of an orbiting brown dwarf (Nakajima et al. 1995) and later a giant planet (Chauvin et al. 2004) via this method. Many more potential companions have since been imaged around other stars (Exoplanet.eu 2013), with the method favouring large objects at wide separations from their hosts. In addition the detection of orbital motion between imaging epochs has allowed constraints to be placed on some companion orbits (e.g. Soummer et al. 2011; Chauvin et al. 2012), with several appearing to have eccentricities significantly greater than zero (e.g. Neuhäuser et al. 2010; Kalas et al. 2013).

Planet formation models generally favour the production of low eccentricity companions, as any eccentricity excitations are quickly damped by the gas disk early on (Lissauer 1993). Gravitational instability is also

thought to initially form protoplanets on low eccentricity orbits (Boss 2011). Therefore the existence of eccentric companions imply some further process occurs beyond formation, which could be planet-planet scattering (Gladman 1993; Marzari & Weidenschilling 2002), 3+ body effects such as secular perturbations (Lee & Peale 2003), stellar flybys (Malmberg et al. 2011) or even planet mergers (Lin & Ida 1997) to name a few mechanisms. An accurate measure of eccentricity is very important for a dynamical understanding of these systems, and an overestimation of this quantity could result in an incorrect understanding of system evolution. A potential source of systematic overestimation of eccentricity in imaged systems is the subject of this paper.

Orbital elements of extrasolar companions detected via any method are generally derived in an astrometric frame (relative to the star) assuming no other bodies in the system. However if an undetected third mass were also present then it would induce a stellar motion about the system barycentre, which could lead to the companion elements derived in this way being incorrect. This

<sup>\*</sup> tdpearce@ast.cam.ac.uk

effect has already been examined for radial velocity (RV) detections; Rodigas & Hinz (2009) showed that 10-20% of RV companions with eccentricities of 0.1-0.4 could actually be on circular orbits with an error introduced by an undetected outer companion, and Wittenmyer et al. (2013) identified several moderately eccentric single planet systems that could be better fitted by two low eccentricity planets. However a similar effect has not been considered for wide separation companions detected by imaging, where an additional mass could lie interior to this object and perturb the stellar motion.

Indeed, the existence of an unseen massive object interior to an imaged companion is often suggested if the latter is on a large eccentric orbit, as the inner mass may be required to scatter the observed object out to such a wide separation (Kalas et al. 2013). In addition, long-term RV trends (e.g. Ségransan et al. 2011) and micro-lensed planets (Gaudi 2012) in some systems suggest that companions at  $\sim 10$  AU may be common, and these objects could have significant masses yet still remain unseen due to limitations in detection methods. High contrast imaging at these separations is difficult and whilst RV surveys have excelled in locating short period companions, detectable planets in Jovian type orbits remain elusive. Furthermore the precision of RV measurements is significantly reduced when applied to young stars due to stellar activity, yet it is in these systems that outer companions are easiest to detect with imaging. This is highlighted by the case of  $\beta$  Pictoris, which shows that massive objects ( $\sim 8M_J$ , where  $M_J$  is the mass of Jupiter) may exist around such stars yet evade RV detection (Lagrange et al. 2009, 2012).

If an unseen massive object existed in a system with a wide separation imaged companion, then this companion could in fact orbit the star-*inner* object barycentre. The motion of the star about this barycentre would then cause the astrometric elements of the imaged companion to vary with a period similar to that of the inner object (e.g. Morbidelli 2002), and hence its observationally derived orbital elements would be incorrect. In this work we examine the effect of such a scenario on the derived eccentricity of the outermost object, which could be over-estimated if an inner companion were present.

The layout of this paper is as follows. Sections 2 and 3 describe the theory work. In Section 2 we consider the case where the observed companion is on a circular barycentric orbit, in order to find the minimum mass of an unseen inner object required to make the outer body appear eccentric. We then generalise this to an eccentric outer companion in Section 3 to find the maximum error in eccentricity which could be induced by an inner object. We suggest criteria to identify systems potentially susceptible to these scenarios in Section 4, and Section 5 provides a step by step method which may be used to evaluate the magnitude of this effect for a given system. We apply this method to Fomalhaut and several other systems as examples. We remark on the detectability of an inner mass in Section 6, and discussion and conclusions are given in Sections 7 and 8.

## 2 OUTER OBJECT ON CIRCULAR ORBIT

### 2.1 Negligible time between observations

Firstly we investigate how an object on a circular barycentric orbit may be given an apparent astrometric eccentricity by an unseen inner companion. We assume that the outer object is small compared to the star, and is sufficiently distant that it undergoes two-body motion about the star-*inner* mass barycentre. We also make the initial assumption that the astrometric position and velocity of the observed companion are both known at a single epoch (i.e. the time between observations required to derive the velocity is negligible compared to the inner object period), which will later be relaxed. Finally the three body system is assumed to be coplanar, though we will later show that any mutual inclination reduces the effect of an inner mass on the astrometric elements of the outer body.

The set-up of this problem is shown on Figure 1. The star and inner object form a circular binary, and the observed companion orbits the binary barycentre. At the moment of observation the barycentric coordinate system is defined to be aligned with the binary separation vector, and the observed object has a true anomaly  $f$  in this frame. We also define an astrometric coordinate system centred on the star, with the axes parallel to those in the barycentric frame. The astrometric position of the observed companion  $\mathbf{r}'$  is therefore given by  $\mathbf{r} - \mathbf{r}_*$ , its barycentric position minus that of the star, and its astrometric velocity  $\mathbf{v}'$  is given by a similar expression. We will use primes to denote astrometric parameters for the remainder of the paper, and the subscript  $i$  will be used to identify parameters associated with the inner object.

We can show that  $\mathbf{r}'$  is given by

$$\mathbf{r}' = a \begin{pmatrix} \cos f \\ \sin f \end{pmatrix} + \mu a_i \begin{pmatrix} 1 \\ 0 \end{pmatrix}, \quad (1)$$

where  $a$  denotes the barycentric outer object semi-major axis,  $a_i$  is the binary separation, and  $\mu \equiv m_i/(m_* + m_i)$  where  $m_i$  and  $m_*$  are the masses of the inner object and star respectively. Additionally the velocity is

$$\mathbf{v}' = \sqrt{\frac{GM}{a}} \begin{pmatrix} -\sin f \\ \cos f \end{pmatrix} + \mu \sqrt{\frac{GM}{a_i}} \begin{pmatrix} 0 \\ 1 \end{pmatrix} \quad (2)$$

where  $M \equiv m_* + m_i$ . To simplify the following we introduce the parameter  $\alpha \equiv a_i/a$  that, along with  $\mu$ , contains all the information required to calculate the astrometric coordinates. The fractional difference between the astrometric and barycentric radii,  $\delta r/r \equiv (r' - r)/r$ , therefore has a maximum absolute value of  $\mu\alpha$ . Similarly,  $\delta v/v = \mu/\sqrt{\alpha}$  at its maximum value. As we only consider unseen companions interior to the observed object,  $\alpha < 1$  so the difference between the astrometric and barycentric radii of the outer object is small whilst the velocity difference may be large. For example, a  $0.01m_*$  object orbiting at  $\alpha = 0.1$  would give the observed companion maximum  $\delta v/v$  and  $\delta r/r$  values of 0.03 and 0.001 respectively.

We convert the astrometric Cartesian coordinates  $\mathbf{r}'$  and  $\mathbf{v}'$  into Keplerian orbital elements, and the resulting semi-major axis and eccentricity are shown as functions

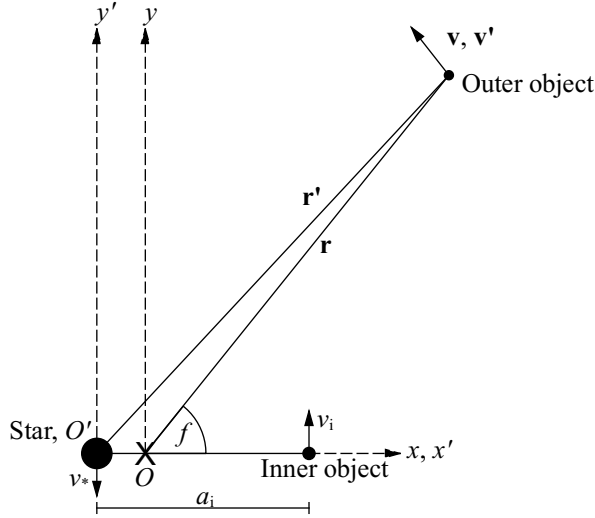


**Figure 1.** Set-up for Section 2.1. The star and inner object form a circular binary of separation  $a_i$  orbiting their barycentre  $O$ . The barycentric frame is centred on  $O$ , with the inner object on the positive  $x$  axis and the star moving in the negative  $y$  direction. The outer object is on a circular orbit about  $O$  in this frame, with a true anomaly  $f$  defined from the  $x$  axis. The astrocentric (primed) frame is centred on the star ( $O'$ ) with the  $x'$  and  $y'$  axes parallel to  $x$  and  $y$  respectively.

of true anomaly  $f$  on Figure 2. The plotted functions are quite cumbersome, but to give the reader a feel for their behaviour we simplify them to the following first order approximations. When  $\alpha$  is small,  $\delta v/v \gg \delta r/r$  and the behaviour of the osculating elements are completely dominated by the velocity shift. In this case the semi-major axis and eccentricity reduce (to first order in  $\mu$ ) to

$$\frac{a' - a}{a} \approx \mu \left[ 1 + \frac{2}{\sqrt{\alpha}} \cos f \right] \quad (3)$$

and

$$e' \approx \mu \left[ 1 + \frac{4}{\sqrt{\alpha}} \cos f + \frac{1}{\alpha} (1 + 3 \cos^2 f) \right]^{\frac{1}{2}}, \quad (4)$$

which are roughly of order  $\mu/\sqrt{\alpha}$ , the same as the velocity shift. These equations provide a very good fit to the full functions, and hence the turning points on Figure 2 may be estimated by substituting  $f = 0, \pi/2$  and  $\pi$  into the above. For example if a companion on a 50 AU circular orbit were observed about a solar type star, an undetected  $10M_J$  object at 1 AU would cause the observed companion's apparent semi-major axis to vary between 43.5 – 57.5 AU and its eccentricity to oscillate between 0.07 and 0.15 with a sub maximum at 0.13.

Note that as  $\alpha$  approaches unity, additional  $\alpha$  terms caused by the radial shift  $\delta r/r$  are no longer negligible in comparison to  $1/\sqrt{\alpha}$ , so Equations 3 and 4 no longer hold. Regardless as we assume the outer object undergoes two

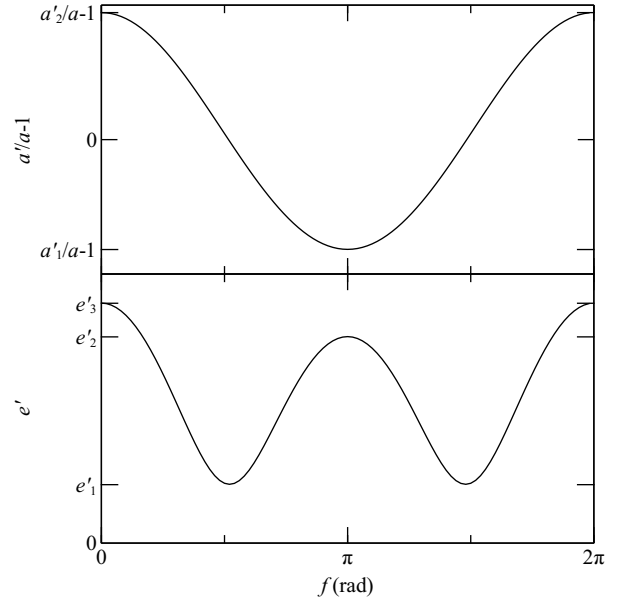


**Figure 2.** Astrocentric semi-major axis and eccentricity of an outer object on a circular barycentric orbit, in the case where the time between observations is small. The turning points of both elements are denoted by subscripts, and may be well approximated by substituting  $f = 0, \pi/2$  and  $\pi$  into Equations 3 and 4. Note that the astrocentric eccentricity is never zero, i.e.  $e'_1 > 0$ . The plots depend only on  $\mu$  and  $\alpha$ , and are qualitatively the same for all parameters.

body motion about the barycentre, the model is invalid in this regime due to three body interactions. However we do not consider such a scenario due to the nature of the problem; as  $\alpha \rightarrow 1$  the mass of this object would have to be large to have any effect and should therefore be detectable. We do not consider  $\alpha > 1$  for the same reason, and additionally the detected companion would be unlikely to orbit the barycentre in this case.

The maximum values of  $\delta r$  and  $\delta v$  occur when  $f = 0$ , i.e. all bodies are aligned, with the star farthest from the outer object. Here the stellar motion opposes the motion of the observed companion, and therefore  $\delta v$  is maximised. We can differentiate the full equations for  $a'$  and  $e'$  and show that these elements are also maximum here. Therefore by substituting  $f = 0$  into the full equation for  $e'$ , we find an upper bound on  $e'$  for each combination of  $\mu$  and  $\alpha$ . This equation may be rearranged to find the minimum value of  $\mu$  (as a function of  $\alpha$ ) required to give the outer object an apparent astrocentric eccentricity  $e'$ . The resulting expression contains terms up to high orders in  $\mu$ , however it may be approximated to better than 5% accuracy by discarding terms greater than second order and multiplying by an empirical factor  $F(e')$  to account for higher order terms. This yields the equation

$$\mu \gtrsim F(e') e' \left[ 1 + 4 \left( \frac{1}{\alpha} + \frac{1}{\sqrt{\alpha}} + \sqrt{\alpha} + \alpha^2 \right) + 2\alpha \right]^{-\frac{1}{2}}, \quad (5)$$

where  $F(e') \equiv (1 + 0.3e')^{-1}$  is the empirically determined factor. Without this factor the above formula overestimates the minimum value of  $\mu$  by  $\sim 25\%$  for high values

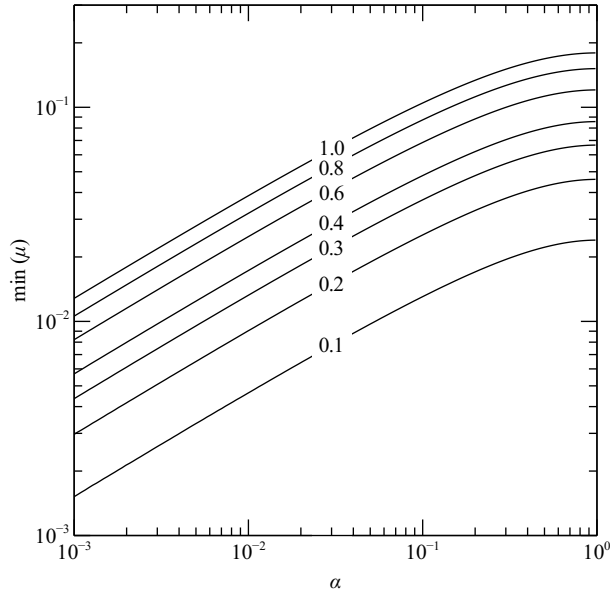


**Figure 3.** Minimum  $\mu$  required to give an outer object on a circular orbit an apparent eccentricity  $e'$ , if the time between observations is much smaller than the inner object period (see Section 2.2 if this is not the case). Each line shows a different  $e'$ . Note the change in behaviour as  $\alpha$  approaches unity as described in the text. This plot is independent of  $m_*$  and  $a$ .

of  $e'$ . The minimum value of  $\mu$  is therefore only dependent on  $\alpha$  and the observed astrometric eccentricity, so is applicable to all systems. Figure 3 shows this minimum mass as a function of  $\alpha$ ; the contours were calculated using the full formalism rather than Equation 5, but are well approximated by the latter. It is clear that the inner mass required to give the outer object a significant apparent eccentricity is generally large, typically in the giant planet to brown/red dwarf regime for a solar type star.

As  $\delta r/r$  is small the approximation  $a \approx r'$  is generally very good, so this may be used to derive  $a_i$  from  $\alpha$ . Also as the minimum value of  $e'$  is non-zero, we could progress in the same way as above to derive an upper limit on inner object mass and thus bound  $\mu$  in  $\alpha$  space. However this limit is not provided as the value is high (such an object would be identifiable using other methods, such as spectroscopy or imaging), so a better upper bound will be given by observational limits.

We have assumed that the three body system is coplanar to derive the above bounds. If this condition is relaxed, we find that any mutual inclination reduces the difference between the two sets of outer object elements. This is to be expected; as noted above, the effect is maximised when the velocity shift  $\delta v$  is greatest, i.e. when the direction of the stellar motion opposes that of the outer body. Mutual inclination reduces the stellar velocity component in the outer companion's orbital plane, and hence lowers the velocity shift and thus its effect on the latter's elements. Therefore the value of  $\mu$  derived using Equation 5 will always be the minimum even if mutually inclined orbits are considered.

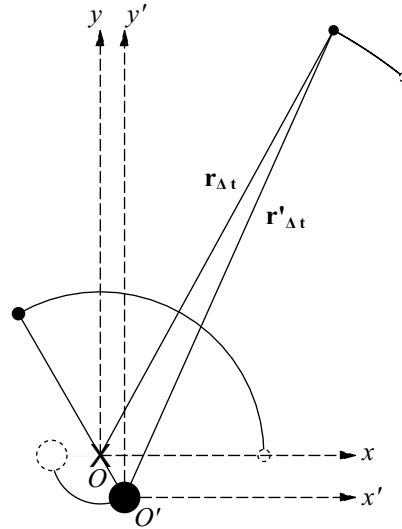


**Figure 4.** Triple system at a time  $\Delta t$  after the first observation. Note that at both epochs the barycentric coordinate system is defined with respect to the inner binary position at  $t = 0$ .

## 2.2 Non-negligible time between observations

Figure 3 suggests that the minimum  $\mu$  required to give a circular companion an apparent eccentricity may always be reduced by placing the inner object ever closer to the star. Unfortunately there is a problem encountered in this regime, as the above assumes that the astrometric coordinates of the outer object are known instantaneously. In reality the velocity is derived by taking (at least) two images at two different epochs, and between these epochs the inner binary has also progressed about its orbit, as shown on Figure 4. The effect of this motion will be significant if the time between observations is of the order of the inner binary period  $T_i$  or greater, so is most important for inner objects on close orbits. It is these objects that were favoured by the previous results, because they suggested that even a small mass at this location could still have a significant effect on the apparent outer companion elements.

We now examine the case where two observations are made at times  $t = 0$  and  $\Delta t$ . All bodies are again on coplanar circular orbits. We assume for simplicity that the time between observations is much smaller than the outer object period, which is valid as companions currently detectable by direct imaging generally exist far from their host star. This means that the motion of the outer object is approximately linear, with velocity  $\mathbf{v}' \approx \Delta \mathbf{r}' / \Delta t$ . Without loss of generality we can specify that at the time of the first observation the system is in the same configuration as for the single epoch case (i.e. the initial outer object position in the astrometric frame is given by Equation 1 with  $f = f_0$ ). At a time  $\Delta t$  later, the observed companion will have a position

$$\mathbf{r}'_{t=\Delta t} = a \begin{pmatrix} \cos(f_0 + \Delta f) \\ \sin(f_0 + \Delta f) \end{pmatrix} + \mu a_i \begin{pmatrix} \cos(n_i \Delta t) \\ \sin(n_i \Delta t) \end{pmatrix} \quad (6)$$

in the new astrometric frame, where  $\Delta f = \sqrt{GM/a^3} \Delta t$  and  $n_i \equiv 2\pi/T_i$ . Therefore we may estimate  $\mathbf{v}'$  as  $(\mathbf{r}'_{t=\Delta t} - \mathbf{r}'_{t=0})/\Delta t$ , and using this and the companion's position in one of the images we may proceed in deriving its astrometric elements as before.

This time the elements are not only functions of  $\mu$  and  $\alpha$  but also of  $\Delta t$ , and the resultant solutions are more complicated than in the previous case. However to first order in  $\mu$  (assuming  $\alpha$  is small) these elements may be well approximated as

$$\frac{a' - a}{a} \approx \mu \left[ 1 + \frac{2}{\sqrt{\alpha}} \zeta(\Delta t) \cos\left(f_0 - \pi \frac{\Delta t}{T_i}\right) \right] \quad (7)$$

and

$$e' \approx \mu \left[ 1 + \frac{4}{\sqrt{\alpha}} \zeta(\Delta t) \cos\left(f_0 - \pi \frac{\Delta t}{T_i}\right) + \frac{1}{\alpha} \zeta^2(\Delta t) \left( 1 + 3 \cos^2\left(f_0 - \pi \frac{\Delta t}{T_i}\right) \right) \right]^{\frac{1}{2}}, \quad (8)$$

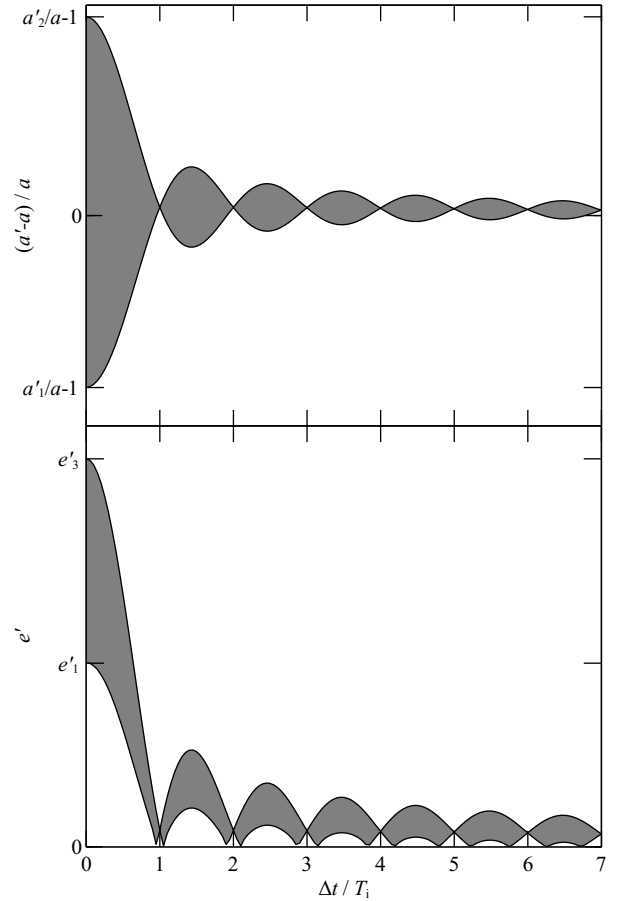
where

$$\zeta(\Delta t) \equiv \text{sinc}\left(\frac{\pi \Delta t}{T_i}\right). \quad (9)$$

Note that in the limit  $\Delta t \rightarrow 0$ ,  $\zeta(\Delta t) \rightarrow 1$  and the above expressions reduce to Equations 3 and 4. The behaviour of these elements as a function of  $\Delta t$  (using the full calculation rather than the first order approximations above) is shown on Figure 5.

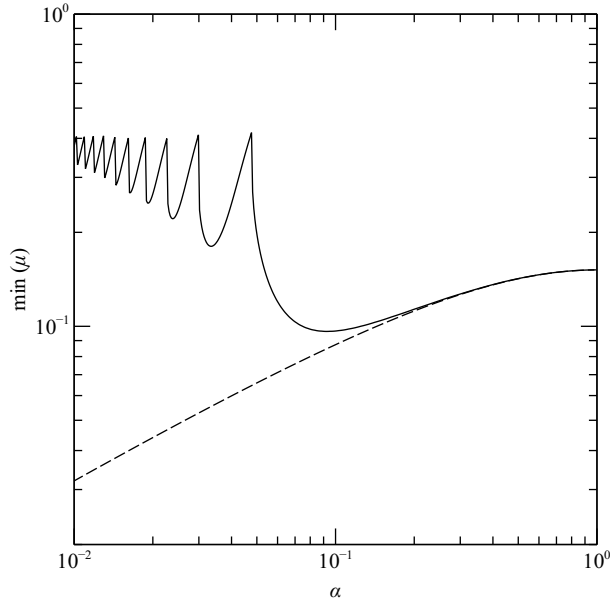
There are several differences between this case and the  $\Delta t/T_i \approx 0$  regime described earlier. Firstly the phases of  $(a' - a)/a$  and  $e'$  are now shifted in  $f_0$  when compared to the single epoch case, due to the changing object positions during the calculation. This manifests itself as the  $f_0 - \pi \Delta t/T_i$  terms in the equations. Secondly the multiple epoch scenario reduces the amplitude of  $(a' - a)/a$  and  $e'$  when compared to the single epoch case; Figure 5 shows that the magnitude of these astrometric elements show a long term decline as  $\Delta t$  is increased. This can be explained by noting that the stellar motion, as well as the motion of the outer object, is effectively averaged by the use of multiple observation epochs. That is, as the observed astrometric velocity is derived as  $\mathbf{v}' = \Delta \mathbf{r}'/\Delta t$  where  $\mathbf{r}' = \mathbf{r} - \mathbf{r}_*$ , the apparent velocity shift caused by the stellar motion is therefore  $\Delta \mathbf{r}_*/\Delta t$ . For circular stellar motion the velocity derived in this way will always be smaller than the true velocity, and so the effect of this averaging is to reduce  $\delta v$  and therefore the amplitude of the outer object's oscillating elements. This manifests itself primarily as the  $T_i/\Delta t$  term in Equation 9, which causes the long term  $\sim 1/\Delta t$  declines in element amplitude visible on Figure 5. Note that if  $\Delta t/T_i > 1$  the inner binary makes at least one complete revolution between observations, and therefore the apparent stellar velocity as “seen” by the outer object will be significantly reduced.

Figure 5 also shows that the elements undergo short



**Figure 5.** Osculating elements as functions of  $\Delta t/T_i$ . For each value of  $\Delta t/T_i$  the astrometric elements oscillate as functions of  $f_0$  (similar to Figure 2), and the range over which they oscillate is denoted here by the shaded region. This plot is system specific and has been produced using  $\mu = 0.001$  and  $\alpha = 0.008$ , but is qualitatively the same for all parameters. The quantities on the vertical axes are the same as on Figure 2; note that the range tends to that of the simpler case as  $\Delta t \rightarrow 0$ .

term oscillatory behaviour as a function of  $\Delta t$ , and that the range over which they oscillate (and hence the dependence on initial outer object true anomaly,  $f_0$ ) is zero when  $\Delta t/T_i$  is an integer. This is another effect of the apparently reduced stellar motion described above. Firstly when  $\Delta t/T_i$  is an integer, the star has the same position at both observation epochs, and so its apparent velocity is zero. As the fractional radial shift  $\delta r/r$  caused by the unseen inner mass is negligible, in this case the outer object effectively “sees” the star with no velocity and very little offset from the barycentre, and so the apparent astrometric elements do not depend on the initial true anomaly of the outer companion. The only difference between the two sets of elements is therefore caused by this small barycentric offset and the use of the star’s mass to derive the astrometric values, rather than the combined mass of the inner binary. Also when  $\Delta t/T_i$  is a half integer (apart from when  $\Delta t/T_i = 1/2$ ) the binary is observed to have advanced by half an orbit, and so  $\Delta \mathbf{r}_*$  and hence  $\delta v$  is maximum. This causes the sub maxima in



**Figure 6.** Minimum  $\mu$  required to give an outer object on a circular orbit an apparent eccentricity of 0.8. The solid line is calculated numerically for the case where the observed companion’s velocity is derived from two observations, and the dashed line shows the single observation regime. Note that this plot is quantitatively system specific and has been produced using  $m_* = 1.92M_\odot$ ,  $a = 120$  AU and  $\Delta t = 7.6$  yrs.

$(a' - a)/a$  and  $e'$  at these locations, although they may be slightly shifted due to the general  $\sim 1/\Delta t$  decline. Note that for  $\Delta t/T_i < 1$  the maxima lies at  $\Delta t/T_i = 0$  rather than  $1/2$ ; this is because the binary has not yet made one complete revolution and so  $\Delta t/T_i \rightarrow 0$  rather than a larger integer, and the apparent stellar velocity therefore tends to its true value. Finally there is a very slight downward trend in  $(a' - a)/a$  as  $\Delta t$  is increased (not very significant in Figure 5 but pronounced in some cases) caused by the breakdown of the linear motion approximation.

The important thing to note for this case is that any non-zero  $\Delta t$  reduces the effect of an unseen inner mass when compared to the single epoch scenario, and that this effect becomes significant if this object lies close to the star. Figure 6 shows the minimum  $\mu$  as a function of  $\alpha$  required to give the outer an astrocentric eccentricity as before, only now for an example set of parameters with  $\Delta t \neq 0$ . The specific masses and turning points are system dependent, however the plot is qualitatively the same for all parameters; at large  $\alpha$ ,  $\Delta t/T_i \rightarrow 0$  and the result tends to the simpler regime of Section 2.1. As  $\alpha$  gets smaller the  $\Delta t \neq 0$  case begins to dominate, and there is now a lower limit on  $\mu$  to give a circular companion an apparent astrocentric eccentricity. Therefore  $\mu$  may not be ever reduced simply by moving the inner object ever closer to the star. Finally the required mass increases sharply beyond this turning point, and sub-minima are also present due to  $T_i$  changing as a function of inner binary semi-major axis.

Proceeding as for the simpler case, we may estimate the minimum unseen mass as a function of  $\alpha$  required

to give an observed circular companion an apparent astrocentric eccentricity  $e'$ . By rearranging Equation 8 we derive an approximate expression for this minimum mass that is valid when  $\mu$  and  $\alpha$  are small:

$$\mu \gtrsim e' \left( 1 + \frac{4}{\sqrt{\alpha}} \zeta(\Delta t) + \frac{4}{\alpha} \zeta^2(\Delta t) \right)^{-\frac{1}{2}}. \quad (10)$$

We may then differentiate this expression with respect to  $\alpha$  and set it to zero to find the absolute minimum value of  $\mu$ . The first non-zero solution to the resulting equation occurs when

$$\tan(\Gamma) = \frac{3}{2}\Gamma, \quad (11)$$

where  $\Gamma \equiv \pi \Delta t / T_i$ .

At this point as no information is known about the unseen inner mass it makes sense to remove the dependence on  $T_i$  from the above equations and replace it with  $\tau$ , the ratio of  $\Delta t$  to the outer object period, which may be more intuitively estimated. Thus  $\Delta t/T_i = \tau/\alpha^{3/2}$  and  $\Gamma = \pi\tau/\alpha^{3/2}$ . Note that all of the system specific information (the star mass,  $\Delta t$  and  $a$ ) is contained within  $\tau$ . As a larger  $\Gamma$  corresponds to a smaller value of  $\alpha$ , the smallest non-zero solution of Equation 11 corresponds to the global minimum value of  $\mu$ .  $\Gamma \approx 0.967$  at this point. Therefore an inner mass will have the greatest effect on the astrocentric elements of the outer if

$$\frac{\Delta t}{T_i} \approx 0.31, \quad (12)$$

i.e. the observational baseline is about a third of the inner object period. Substituting this into Equation 10, we find that in order for an unseen inner mass to give a circular outer object an astrocentric eccentricity  $e'$

$$\mu \gtrsim e' \left( 1 + 2.30\tau^{-1/3} + 1.32\tau^{-2/3} \right)^{-\frac{1}{2}}, \quad (13)$$

and the location of this mass in order for  $\mu$  to have the minimum possible value must be

$$\alpha \approx 2.19\tau^{2/3}. \quad (14)$$

The latter equation is independent of  $e'$ , and so the radius at which the inner object has the greatest effect is only dependent on  $a$  and  $\tau$ . The secondary minima on Figure 6 correspond to higher  $\Gamma$  solutions to equation 11, and the peaks correspond to a second set of  $\alpha$ -dependent roots to the differential of Equation 10. Whilst the above equations are only approximate, they agree well with minimum masses and corresponding semi-major axis ratios calculated numerically without any simplifications.

Figure 7 shows the absolute minimum  $\mu$  as a function of  $\tau$  and  $e'$  calculated by a numerical grid search, which shows good agreement with Equation 13 for  $\tau \lesssim 10^{-2}$ . Above this value the two diverge as the linear motion approximation breaks down; assuming the companion moves in a straight line between epochs will always introduce an error on the derived elements, and this error will increase as a greater fraction of the orbit is observed.

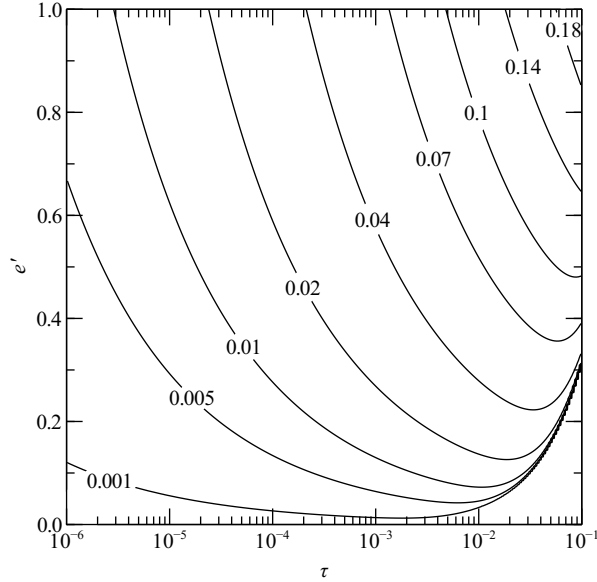


**Figure 7.** Minimum  $\mu$  required to give an outer object on a circular orbit an apparent eccentricity  $e'$ , as a function of  $\tau$ . The graph was calculated numerically without making any approximations, but shows good agreement with Equation 13 for  $\tau \lesssim 10^{-2}$ . Above this value the lines of arbitrary  $\min(\mu)$  converge, as the error on the eccentricity caused by the assumption that the companion motion is linear becomes more significant than the error caused by an unseen mass.

Therefore this effect is most apparent in the lower right corner of the plot, where the difference between the outer object's true velocity and that estimated linearly is sufficient to give the body an apparent eccentricity even in the absence of a third mass. This plot may be used to establish whether the apparent eccentricity of an observed companion could be entirely caused by the presence of an unseen inner mass.

The parameter  $\tau$  is given by

$$\tau = \frac{\Delta t}{2\pi} \sqrt{\frac{G(m_* + m_i)}{a^3}} \quad (15)$$

and contains two unknowns,  $m_i$  and  $a$ . However we again take advantage of  $\delta r/r$  being small, and hence can make the approximation  $r' \approx a$ . Therefore  $\tau$  may be accurately estimated as

$$\tau \approx \Delta t \sqrt{m_*} r'^{-3/2}, \quad (16)$$

where  $m_*$ ,  $\Delta t$  and  $r'$  are in units of solar masses, years and AU respectively. This approximation may be used in all of the above calculations. As an example suppose two observations of an object at 100 AU from a solar type star are made 1 year apart, and orbital motion is detected between the epochs yielding an astrometric eccentricity of 0.5. If the object is actually on a circular orbit then  $\tau = 10^{-3}$ , and thus from Figure 7 we see that  $\min(\mu)$  is between 0.02 and 0.04 (the actual value is 0.035). Equation 14 shows that in order for  $\mu$  to have this minimum value, the inner body must be located at 2.2 AU.

### 3 OUTER OBJECT ON ELLIPTICAL ORBIT

We now generalise the above results to allow the outer object to have some eccentricity in the barycentric frame. As before an inner mass could potentially increase this eccentricity in the astrometric frame. The apparent eccentricity may also now be decreased, i.e. an unseen mass could also make the companion appear less eccentric than it actually is. However as circular orbits are generally favoured by planet formation models and highly eccentric companions point towards some disruptive dynamical event in the system's history, we only focus on increasing the companion's apparent eccentricity in this paper. The magnitude of this effect is expected to be roughly symmetrical, so an unseen mass could potentially increase or decrease the apparent eccentricity of an imaged companion by roughly the same amount. Therefore the size of the potential eccentricity underestimation may also be estimated by the following method.

#### 3.1 Negligible time between observations

We will proceed as before, by first analysing the  $\Delta t = 0$  regime and then extending this to the multiple epoch case. We again assume the orbits to be coplanar, and the inner binary orbit is still circular. Equations 1 and 2 now become

$$\mathbf{r}' = \frac{a(1-e^2)}{1+e\cos(f)} \begin{pmatrix} \cos(\omega+f) \\ \sin(\omega+f) \end{pmatrix} + \mu a_i \begin{pmatrix} 1 \\ 0 \end{pmatrix} \quad (17)$$

and

$$\mathbf{v}' = \sqrt{\frac{GM}{a(1-e^2)}} \begin{pmatrix} -\sin(\omega+f) - e\sin\omega \\ \cos(\omega+f) + e\cos\omega \end{pmatrix} + \mu \sqrt{\frac{GM}{a_i}} \begin{pmatrix} 0 \\ 1 \end{pmatrix}, \quad (18)$$

where  $e$  is the barycentric eccentricity. As for the  $e = 0$  case, we use these equations to derive the outer object's astrometric elements. The system now has a 2D phase, given by the argument of periapsis ( $\omega$ ) and  $f$ . The change in elements is maximised when the difference between the stellar motion and that of the outer body is greatest, which occurs when the outer object is at pericentre. The maximum values of  $a'$  and  $e'$  therefore occur when  $\omega = f = 0$ . Proceeding as before we may again derive a lower limit on the unseen inner mass based on the observed companion's astrometric eccentricity, which now depends on its assumed barycentric eccentricity.

Figure 8 shows the maximum fractional error in observed eccentricity,  $\Delta e/e' \equiv (e' - e)/e'$ , as a function of  $\mu$  and  $\alpha$  for different observed astrometric eccentricities. Note that if  $\Delta e/e' = 1$  then the outer object is on a circular orbit, and also that the errors plotted are positive (i.e.  $e' > e$ ). The contours were again calculated using the full expression and we also derive a simplified analytical expression equivalent to Equation 10, but it is cumbersome and so given in the appendix. Figure 8 is analogous to Figure 3 as they are both independent of star mass and semi-major axes.

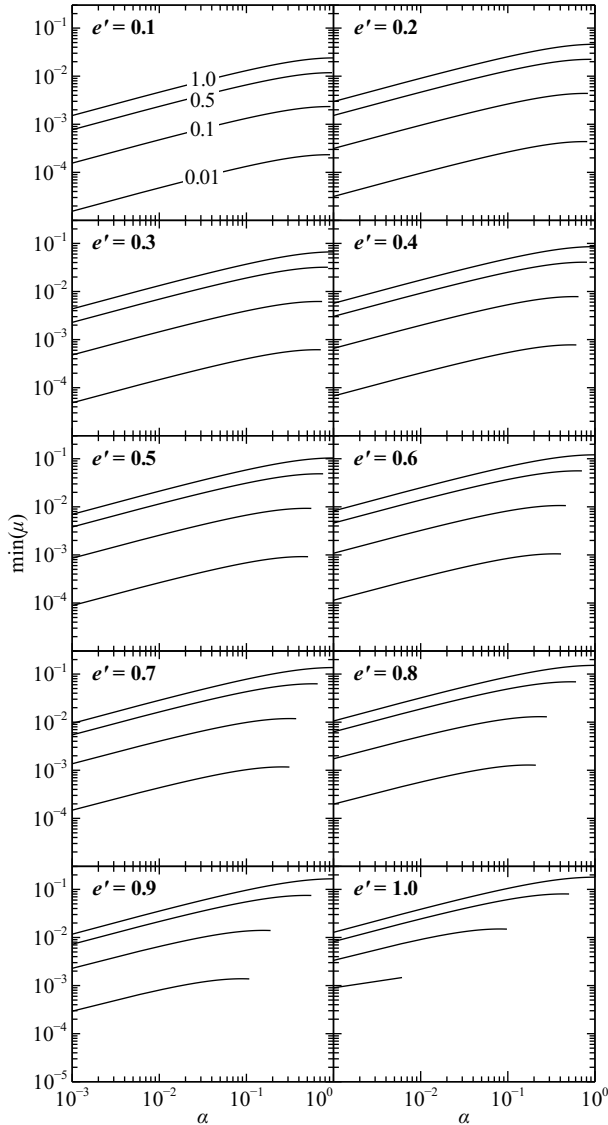


**Figure 8.** Minimum  $\mu$  required to induce a given fractional error in observed eccentricity,  $\Delta e/e' \equiv (e' - e)/e'$ , as a function of  $\alpha$  for different astrocentric eccentricities in the  $\tau = 0$  regime. The lines show  $\Delta e/e' = 0.01, 0.1, 0.5$  and  $1.0$  in the order shown on the  $e' = 0.1$  panel, and may be estimated using the equation in the Appendix. The model is not valid if the outer object is inside the orbit of the inner at pericentre, so the values of  $\alpha$  resulting in this scenario are omitted. For an observed  $e'$ , the reader may use this plot to determine the maximum error on the derived eccentricity given observational upper limits on  $\mu$  as a function of  $\alpha$ .

The plot is qualitatively similar to Figure 3, as  $\min(\mu)$  still follows a  $\sqrt{\alpha}$  dependence and turns over as other  $\alpha$  terms become non-negligible. We have neglected orbits for which the outer companion has pericentre interior to the orbit of the inner mass, as 3 body dynamics would also be important in this region and the results would be incorrect. As for Figure 3, this plot may be used to determine the maximum error on the derived eccentricity of a companion, given an observational upper limit on the inner mass as a function of orbital radius.

### 3.2 Non negligible time between observations

Once again, we consider the use of multiple observational epochs to derive the outer companion velocity. All analytics are now very inelegant and can be sensitive to simplifications, so there is little merit in reproducing them here. However the resulting plots of  $\min(\mu)$  required to boost  $e$  up to  $e'$  as a function of  $\alpha$  are qualitatively the same as Figure 6, but shifted down slightly as  $\min(\mu)$  does not have to be as large. Figure 6 is *not* shifted in  $\alpha$  by the introduction of non-zero  $e$ , i.e. the global minimum value of  $\min(\mu)$  still occurs at the same ratio of semi-major axes as the  $e = 0$  case. This has been tested numerically across the entire parameter space. Therefore Equation 14 may still be used to locate the value of  $\alpha$  where the inner mass will have the greatest effect, although Equation 13 no longer holds.

As the introduction of multiple observations again leads to an absolute minimum value of  $\mu$  required to give an outer object a given astrocentric eccentricity, we may produce a plot analogous to Figure 7 that shows this minimum mass as a function of  $\tau$ . This is presented on Figure 9 for various astrocentric eccentricities, found using a numerical grid search. Note that the behaviour for  $\tau \gtrsim 10^{-2}$  is similar to that on Figure 7 due to the breakdown of the linear motion approximation.

This plot may be used to establish whether the apparent eccentricity of an observed companion could be incorrect due to the effect of an unseen inner mass. However there is one final problem; if the outer object may now have a barycentric eccentricity, we can no longer approximate the parameter  $\tau$  in the same way as before because the barycentric semi-major axis is unknown. However we may constrain  $\tau$  to lie along a line in  $\Delta e/e'$  space for the best case scenario, so we can still find the minimum inner mass required to introduce a given error on the outer object eccentricity. As  $\tau$  will be small for wide separation companions, the greatest change in orbital elements will occur if this body is near pericentre. In addition we know that  $\delta r/r$  is small, so at this point  $r' \approx a(1 - e)$ . Hence replacing  $a$  with  $[m_* (\Delta t/\tau)^2]^{1/3}$  will give the value of  $\tau$  if the object is at pericentre, which is a function of  $e$ . Noting that  $e = e'(1 - \Delta e/e')$  we can then rearrange this in terms of  $\Delta e/e'$ . Therefore if the outer object is at pericentre then

$$\frac{\Delta e}{e'} \approx 1 + \frac{r'}{e'} \left[ \frac{1}{m_*} \left( \frac{\tau}{\Delta t} \right)^2 \right]^{1/3} - \frac{1}{e'}, \quad (19)$$

where  $m_*$ ,  $\Delta t$  and  $r'$  are again in units of solar masses, years and AU respectively. This equation may be overplotted on the appropriate panel of Figure 9, and hence the maximum eccentricity error an unseen mass may introduce will be at the  $\Delta e/e'$  value where this mass contour crosses the above line.

We plot line this for an example set of parameters on Figure 10, along with the appropriate panel of Figure 9. For many systems, such as that plotted here, the possible range of  $\tau$  will only span about an order of magnitude and so can be estimated fairly easily. A similar plot may be made by the user for their system of interest, and should



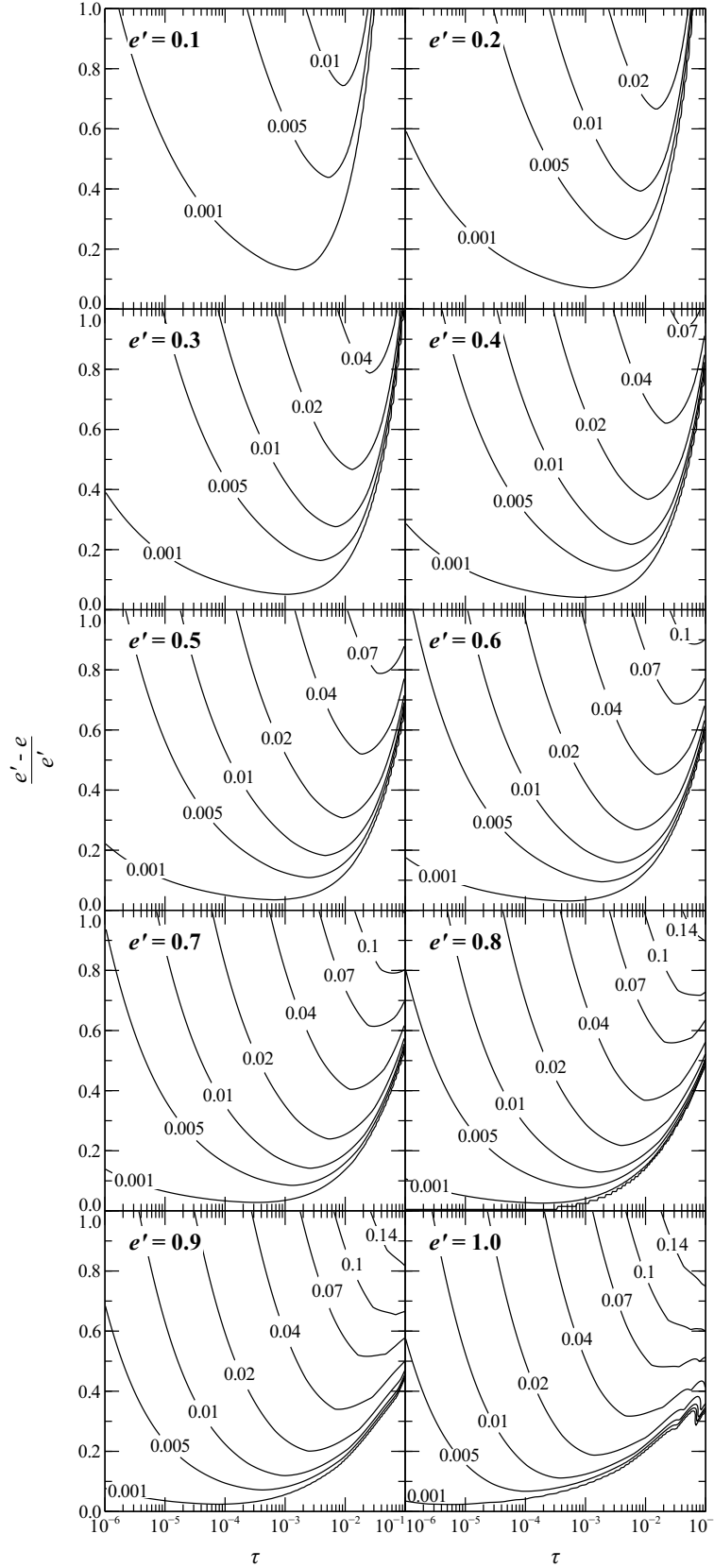


**Figure 9.** Minimum  $\min(\mu)$  required to induce a given fractional error in observed eccentricity,  $\Delta e/e'$ , as a function of  $\tau$  for different astrocentric eccentricities. The values of  $\alpha$  corresponding to these minimum masses may still be found using Equation 14. Note the deviations from smooth contours on the right side of the  $e' = 1.0$  plot are numerical in nature, and should be ignored.

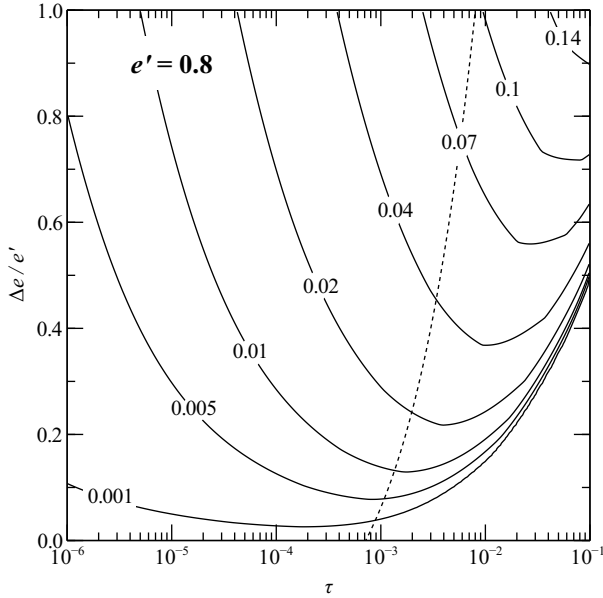


**Figure 10.** Example application of  $\tau$  constraining using Equation 19, with the parameters  $m_*$ ,  $\Delta t$ ,  $r'$  and  $e'$  equal to  $1.92M_\odot$ , 7.6 yrs, 120 AU and 0.8 respectively. The maximum possible error in orbital elements for a given inner mass occurs where this contour crosses the dotted line (Equation 19). For example if the maximum permitted  $\mu$  is 0.04, then the maximum fractional error an inner mass could induce on the eccentricity would be 0.45.

be used to establish whether an unseen inner mass could introduce a significant error on the outer eccentricity.

#### 4 APPLICABILITY

The scenario outlined in this paper, in which a directly imaged companion has incorrectly derived orbital elements due to the effect of an unseen inner mass on the stellar motion, will not be important for all directly imaged systems. In this section we examine what criteria a system must fulfil in order for this scenario to warrant consideration.

We require the system to harbour a directly imaged companion for which orbital motion has been detected, which is also much less massive than its parent star. We also require the parameter  $\tau$  to be small in order for the inner body to have the greatest effect; Figures 7 and 9 show that  $\tau$  must also be of order  $10^{-2}$  or smaller if the primary effect on  $e'$  is to be caused by an inner mass rather than a breakdown of the linear motion assumption. However there are bounds on the minimum value of  $\tau$  for a given system, set by observational limitations. Firstly  $\Delta t$  may not take any arbitrary value; in reality we have a maximum observational baseline,  $\max(\Delta t)$ . Substituting this into the equation for  $\tau$ , we arrive at an upper limit of

$$\tau < \max(\Delta t) \sqrt{\frac{m_*}{a^3}} \quad (20)$$

where  $\max(\Delta t)$ ,  $m_*$  and  $a$  are in units of years, solar

masses and AU respectively. There is also a lower limit on  $\tau$ , which arises because the difference in the angular separation of the companion between the two observational epochs must be large enough to be resolvable. If the orbit of this object is eccentric, then the largest change in angular position will occur if the orbit is face on with the object at pericentre. If  $\tau$  is small, we may approximate the change in true anomaly to be  $\Delta f \approx 2\pi\tau\sqrt{(1+e)/(1-e)^3}$  at this point. Between the two epochs the companion will move by an angular distance of approximately  $[a(1-e)/d]\Delta f$  at pericentre as viewed from Earth, where  $d$  is the distance to the system. Therefore the lower bound on  $\tau$  is given by

$$\tau > \frac{3\sqrt{2}\theta_{\text{cen}}}{2\pi} \sqrt{\frac{1-e}{1+e}} \frac{d}{a}, \quad (21)$$

where  $\theta_{\text{cen}}$  is the  $1\sigma$  half width centroiding accuracy. The factor of  $3\sqrt{2}$  comes from the requirement of a three sigma detection of orbital motion. If  $\theta_{\text{cen}}$  is in radians then  $d$  and  $a$  must be in the same units; alternatively if  $\theta_{\text{cen}}$  is in arcseconds then  $d$  and  $a$  are in parsecs and AU respectively.

The above equations show that for this scenario to be potentially important the observed system must be nearby (small  $d$ ) with a wide separation companion, but not so wide that orbital motion is undetectable. Eliminating  $\tau$  from the above equations, for orbital motion to be detected the semi-major axis must fulfil

$$a < m_* \frac{1+e}{1-e} \left( \frac{2\pi \max(\Delta t)}{3\sqrt{2}\theta_{\text{cen}}d} \right)^2 \quad (22)$$

(again,  $3\sqrt{2}$  comes from the requirement of a three sigma detection of orbital motion).

Additionally an absolute lower limit on  $a$  is  $d\theta_{\text{res}}/2$ , where  $\theta_{\text{res}}$  is the full width instrument angular resolution. This arises from the observable star-companion separation, and is not  $m_*$  or  $e$  dependent. This is a lower bound because in general the detection of companions close to the star is contrast limited as opposed to resolution limited. Therefore only very massive companions may be observed down to the ‘‘currently unresolvable’’ limit, and lower mass objects must lie farther out to be detected. For example whilst the resolution of the HST is  $0.2''$ , its effective inner working angle is actually about  $0.7''$  in the infrared (Krist 2006). The dependence of detectability on mass is not an issue for the outermost companions in this paper, because the analysis presented here is independent of this quantity provided that the imaged object is not massive enough to significantly perturb the inner binary. However this dependence will affect our ability to detect an inner object, as even a significant mass may be lost in the glare of the star if its semi-major axis is small enough (see Section 6).

Figure 11 shows all of the above limits on  $a$  as functions of  $d$  for the  $e = 0$  case, as well as the maximum and minimum values of  $\tau$  from Equations 20 and 21. We assume a maximum baseline of 10 yrs and a resolution of  $0.2''$ , that of the HST, for the above equations. The centroiding accuracy is taken to be  $0.01''$ , which may be reached by current observations (e.g. Golimowski et al.

1998; Kasper et al. 2007; Neuhäuser et al. 2008, 2010). In fact some observations have achieved even better accuracies, however we will use  $0.01''$  as a typical value because we feel it is a better representation of the current level of precision. We also plot the projected separations and distances for a selection of sub-stellar companions detected by imaging (compiled from Reid et al. 2001; Wilson et al. 2001; Metchev & Hillenbrand 2004, 2006; Chauvin et al. 2005; Zuckerman & Song 2009; Tanner et al. 2010; Rodriguez et al. 2012 and Exoplanet.eu 2013). Companions with probable ( $\geq 3\sigma$ ) and possible detections of orbital motion are highlighted, and we give details of these objects in Table 1. This should give the reader a feel for the region of parameter space occupied by these objects, in relation to that which may be important for the scenario described in this paper. Note that we have not plotted the astrometric semi-major axes of the companions; we assume nothing about their orbits or orientations. However the projected separations should provide order of magnitude approximations of  $a$  sufficient for this plot.

As already stated, the effect of an inner mass on the derived elements of an outer companion will be most important if  $\tau$  is small. This condition means that systems most susceptible to this effect would lie as high up Figure 11 as possible (but below the upper limit for detectable orbital motion). Figures 7 and 9 suggest that  $\tau \lesssim 10^{-2}$  for the inner body to significantly affect the derived elements of the outer body. It is clear that the area of parameter space where this scenario could be applicable is well populated by companions, so could be important for around half of currently imaged systems. Also note that the solid line scales as  $(\max(\Delta t)/\theta_{\text{cen}})^2$ , so as observational techniques improve and achieve longer time baselines, more objects could be discovered that would be susceptible to this scenario.

The next generation instruments GPI and SPHERE (Macintosh et al. 2006 and Dohlen et al. 2006 respectively) are expected to discover many companions within 100 AU of young stars at 30 - 50 pc. Whilst not populating the upper regions of Figure 11, many of these objects could still be susceptible to eccentricity errors caused by unseen inner masses. Furthermore as better centroiding precisions are achieved by these projects and others, orbital motion will be detectable using observations covering smaller fractions of companion orbits. This means that lower  $\tau$  values will be reached, and hence these objects would be more susceptible to eccentricity errors induced by unseen inner masses. Therefore we conclude that the effect described in this paper could already be significant for many directly imaged systems, and will be applicable to more imaged companions in the future.

## 5 HOW TO USE THIS PAPER

### 5.1 Suggested Method

In the above three sections we described the set-up of the problem. We now suggest a step-by-step method to establish whether a derived astrometric eccentricity is likely

to be incorrect due to the presence of an inner object. We then apply this method to some example systems.

(i) Is the system suitable? It should have a known stellar mass and at least two images of the companion, between which orbital motion is observed. The user should also have estimates of the de-projected companion-star separation  $r'$  and astrometric eccentricity  $e'$ . If the inclination is unknown then a lower bound on this eccentricity may be derived by varying the assumed line of sight position and velocity until a minimum is found. If the stellar rotation axis is known then the inclination may be estimated by assuming that the star and companion are coplanar (e.g. Le Bouquin et al. 2009; Watson et al. 2011; Kennedy et al. 2013). The system should also lie above the horizontal  $\tau < 10^{-1}$  line on Figure 11.

(ii) Could the companion be on a circular barycentric orbit? To establish this, estimate  $\tau$  using Equation 16 and find the minimum inner mass required to give the observed  $e'$  using Figure 7. Calculate the semi-major axis of this mass using Equation 14; if an object with this mass and location cannot be ruled by observation then it is possible for the imaged object to be on a circular orbit about the star-inner mass barycentre. If the inner mass is observationally excluded in this region but a larger mass may exist further out, use Figure 3 or Equation 5 to see if this object may lie farther from the star. Remember that these relations are not valid all the way up to  $\alpha = 1$  due to three body dynamics. Also note that the mass may exist closer in than the Equation 14 value, but as the required mass rises steeply with decreasing distance (Figure 6) this is a less useful consideration.

(iii) If the companion must be eccentric, what is the maximum error in this barycentric eccentricity that could be caused by an inner body? Firstly estimate  $\tau$  as a function of  $\Delta e/e'$  using Equation 19, similar to that plotted on Figure 10. Locate the graph on Figure 9 that corresponds to the observed value of  $e'$ , and overlay this  $\tau$  constraint onto it. For each combination of  $\min(\mu)$  and  $\tau$  that lies in along this line establish whether such an inner mass could exist at a distance given by Equation 14, noting that  $a$  will have to be estimated as  $r'/(1-e)$ . If it may, then use Figure 9 to read off the maximum eccentricity error  $\Delta e/e'$  corresponding to this combination of  $\tau$  and  $\min(\mu)$ . Again, if the inner object cannot exist in this region but a larger mass cannot be excluded further out, use Figure 8 or the equation in the appendix to calculate this minimum mass.

If an observer wishes to minimise the effect of this scenario on a system, the best technique would be make multiple observations over a long baseline. This would increase  $\tau$  and thus reduce the average stellar velocity. The use of more than two observations would also reduce the effect of the third body, as the observed astrometric elements would oscillate over time and so would vary depending on the pair of observations used to derive them. This could be used in some cases to exclude inner masses with periods shorter than the longest baseline.

Companion	$d$ (pc)	Projected Separation (AU)	Reference
Probable ( $\geq 3\sigma$ ) detection of orbital motion			
2M 0103(AB)-b	$47 \pm 3$	$84 \pm 5^a$	Delorme et al. (2013)
$\beta$ Pic-b	$19.44 \pm 0.05$	$8.3 \pm 0.3$	Chauvin et al. (2012)
Fomalhaut-b	$7.70 \pm 0.03$	$103.2 \pm 0.5$	Kalas et al. (2013)
Gl 229-B	$5.77 \pm 0.04$	$44.3 \pm 0.3$	Golimowski et al. (1998)
HR 7672-B	$17.8 \pm 0.1$	$9.2 \pm 0.1$	Crepp et al. (2012)
HR 8799-b	$39 \pm 1$	$68 \pm 2$	Marois et al. (2008)
-c	-	$38.0 \pm 1.0$	-
-d	-	$24.5 \pm 0.6$	-
-e	-	$14.6 \pm 0.4$	Marois et al. (2010)
PZ Tel-B	$52 \pm 3$	$20 \pm 1$	Mugrauer et al. (2012)
TWA 5-B	$44 \pm 4$	$86 \pm 2^a$	Neuhäuser et al. (2010)
Possible ( $< 3\sigma$ ) detection of orbital motion			
$\eta$ Tel-B	$48 \pm 2$	$200 \pm 6$	Neuhäuser et al. (2011)
GJ 504-b	$17.56 \pm 0.08$	$43.9 \pm 0.5$	Kuzuhara et al. (2013)
GQ Lup-B	$150 \pm 50$	$110 \pm 40$	Neuhäuser et al. (2008)
GSC 0621400210-b	$150 \pm 10$	$320 \pm 30$	Ireland et al. (2011)
HD 130948-B, -C	$18.2 \pm 0.1$	$47.3 \pm 0.3^b$	Ginski et al. (2013)

**Table 1.** Distances and projected separations for a selection of imaged sub-stellar companions for which orbital motion may have been detected. <sup>a</sup>Central object is a multi-star system, and companion separation is given from the system barycentre. <sup>b</sup>Companion is a binary, and separation is given from the central mass to the binary barycentre.

## 5.2 An example: the Fomalhaut system

Figure 11 shows that the area of separation-distance parameter space where an unseen inner mass could affect the derived eccentricity of an observed object is well populated by companions. However orbital motion has not been detected for many of these objects as the required observations have yet to be made. If additional measurements are taken in the near future, for example in an attempt to build up an exoplanet/brown dwarf eccentricity distribution, then the presence of unseen masses could induce significant errors on this distribution. However until such measurements are made the most susceptible planetary system is Fomalhaut, which we will use here as an example to demonstrate the above method.

The star has a mass of  $1.92M_{\odot}$ , with a directly imaged planet (Fomalhaut-b) at 100 AU in projection for which orbital motion has been observed over four epochs between 2004 and 2012 (Kalas et al. 2013).  $\tau$  therefore lies between  $10^{-4}$  and  $10^{-2}$  from Figure 11. The system also contains a narrow debris disk (Kalas et al. 2005); if the planet is assumed to lie in the plane of this disk then its astrometric position and velocity are  $\sim 120$  AU and  $\sim 1$  AU/yr respectively, yielding an astrometric eccentricity of about 0.8 (Kalas et al. 2013). Thus this system is suitable for the method outlined in this work.

We first test the hypothesis that the planet’s orbit is actually circular in a barycentric frame and is aligned with the disk. Using Equation 16 with  $\Delta t = 7.6$  yrs we calculate  $\tau$  to be 0.008. Figure 7 shows that for Fomalhaut-b to be on a circular orbit with an inner mass giving it an astrometric eccentricity of 0.8, the unseen inner companion must have  $0.07 < \min(\mu) < 0.1$  for this value of  $\tau$ . Equation 14 shows that such a planet would exist at  $\alpha = 0.09$ , and therefore  $a_i = 11$  AU. Such a planet is ruled out by photometric non-detections (Kenworthy et al. 2009, 2013), which place a model dependent upper

mass limit for  $a_i > 5$  AU of  $12 - 20M_J$  ( $\mu \sim 0.006 - 0.01$ ). This limit is an order of magnitude lower than required, so Fomalhaut-b cannot be on a circular orbit coplanar with the disk with its apparent eccentricity caused by an inner planet.

We now relax the condition that Fomalhaut-b must lie in the disk plane, to establish whether it is possible for the companion to have a circular orbit in any orientation. By varying the assumed line of sight position and velocity components of the companion we derive a lower bound on its astrometric eccentricity, which is 0.5–0.8 depending on the pair of observation epochs used. If we assume the orbital plane that gives  $e' = 0.5$ , then  $a = 166$  AU and  $\Delta t = 1.7$ . Therefore  $\tau = 0.001$ , and Figure 7 shows us that in order for Fomalhaut-b to be circular with this apparent eccentricity  $\min(\mu)$  must be between 0.02 and 0.04. This is still higher than the upper bound from observations, and so Fomalhaut-b has a barycentric eccentricity regardless of the chosen orbital plane.

Given that the orbit of Fomalhaut-b cannot be circular, we now wish to establish the maximum error in its barycentric eccentricity that could be caused by an observationally allowed unseen mass. We revert to the case where the planet and disk are coplanar. We first use Equation 19 to constrain  $\tau$  as a function of barycentric eccentricity, as we may no longer estimate  $\tau$  using Equation 16 because we have no information about the true semi-major axis. Note that Equation 19 again assumes the companion to be at pericentre as this is the most favourable case for the scenario described in this paper. We overlay this  $\tau$  constraint on the  $e' = 0.8$  plot from Figure 9, which is shown for the relevant parameters on Figure 10. We know from the observational upper limits that  $\mu \leq 0.006$ , so the maximum value of  $\Delta e/e'$  that this mass may induce occurs when the  $\tau$  constraint intersects the  $\mu = 0.006$  contour. This is at  $\Delta e/e' = 0.088$ , which

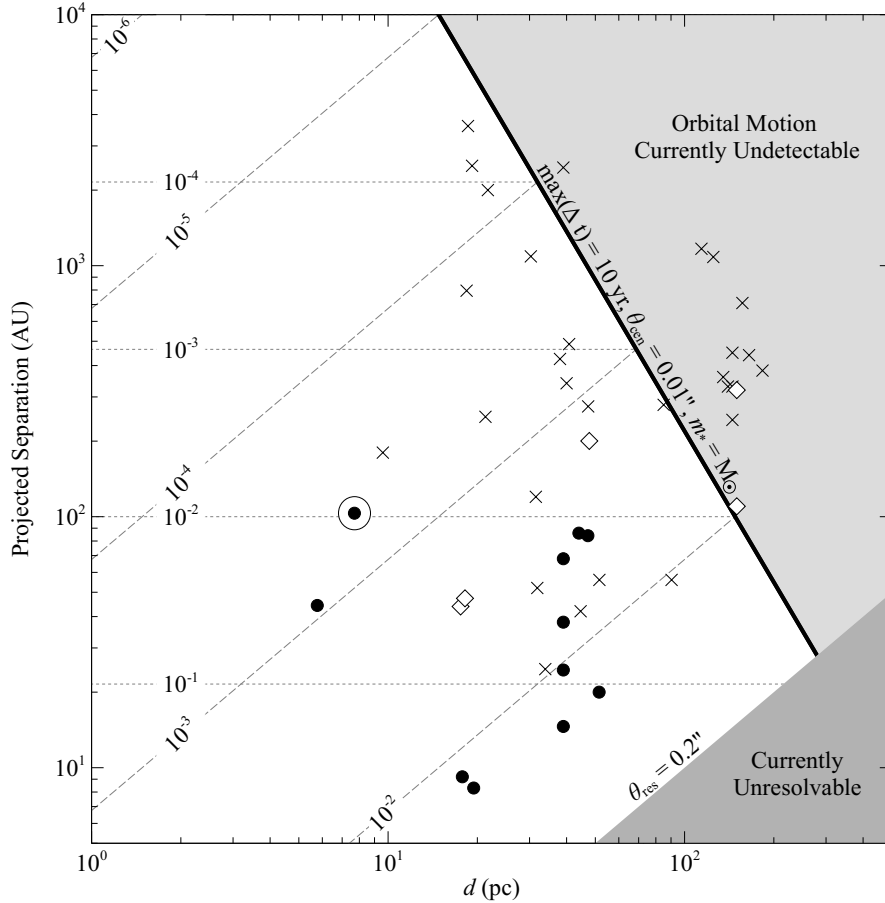


**Figure 11.** Projected separations of directly imaged sub-stellar companions. Circles and diamonds denote objects with probable ( $\geq 3\sigma$ ) and possible detections of orbital motion respectively. Crosses show companions with measured orbital motions consistent with zero. The two shaded regions show the areas where companions are currently unresolvable and where orbital motion is usually too small to be detected, both derived using parameters typical of modern observations. The two companions lying in the latter region with possible detections of orbital motion have unusually good centroiding accuracies of  $\sim 1$  mas, and motion has not been detected to  $3\sigma$ . Note that the minimum separation required for detection will be higher than the limit from resolution alone due to contrast effects, but not by enough to affect the conclusions of this work. The diagonal dashed and horizontal dotted lines show the minimum and maximum values of  $\tau$  respectively, for  $1M_{\odot}$  stars using a 10 yr baseline (Equations 20 and 21). For example, if Fomalhaut-b (circled) were on a circular orbit,  $\tau$  would lie between  $10^{-2}$  and  $10^{-4}$ . A lower  $\tau$  indicates a higher susceptibility to the scenario described in this paper (see Figures 7 and 9).

corresponds to  $e \geq 0.73$ . Therefore using Equation 12 we see that a  $12M_J$  mass at  $a_i = 10$  AU could introduce a 10% error on Fomalhaut-b's eccentricity.

Note that as we have four observations of Fomalhaut-b, we know that the linear velocity approximation is still good over at least eight years. Even though the inner planet / brown dwarf described above would have a period of about twenty years, we cannot use b's constant velocity to rule out such an object because the changing velocity of the star itself would be undetectable; the star would have moved by about  $2\mu\alpha a = 0.1$  AU ( $0.01''$  at 7.7 pc) over eight years, which would change the planet's velocity by 1% and would therefore be undetectable with the current precision. Furthermore the uncertainties in  $e'$  from the astrometry and assumptions about the orbital plane are large enough that the use of more than one pair of observations cannot rule out the scenario outlined above. We therefore conclude that, whilst Fomalhaut-b cannot be on a circular barycentric orbit, an unseen  $12$

$M_J$  companion at 10 AU could result in a  $\sim 10\%$  overestimation of its astrocentric eccentricity, so it serves as a good example of a possible use of the above method.

### 5.3 Other example systems

In addition to Fomalhaut-b, we also applied the method to other applicable systems from Table 1. We excluded  $\beta$  Pic-b as its  $\tau$  value is too high, and HR7672-B due to RV constraints on the inner mass. We also excluded the 2M 0103(AB), HR 8799 and TWA 5 systems from analysis as they are known to host more than one companion, and the current method is therefore unsuitable. Note however that we do include HD 130948, in which the companion itself is a known binary, by treating the pair as a single object.

All of these companions have orbital motion which appears linear over the observational baseline, and their sky plane positions and velocities were therefore derived

by fitting linear trends. However unlike Fomalhaut, the majority of these systems do not have any additional information with which to predict the plane of the companion's orbit.  $\eta$  Tel does have a debris disk which is close to face on, so if the companion / disk are aligned then the former may be assumed to orbit in the sky plane (Smith et al. 2009). However it is not clear that the two objects should necessarily be aligned, as the companion lies much farther from the star than the disk. Therefore we derive astrometric eccentricities for all companions in two extreme cases. In the first case we assume that the orbit is constrained to the sky plane, and in the second case we assume that the orbit is orientated in such a way that the astrometric eccentricity is minimised. Assuming the companions are actually on circular orbits, we calculate the locations and masses of the lightest inner objects required to give the observed eccentricities. The results are shown in Table 2.

Firstly we consider the case where the orbits are assumed to lie in the sky plane. Four of these companions (Gl 229-B, GJ 504-b, GQ Lupi-B and GSC 06214-00210-b), in spite of their high astrometric eccentricities, could actually be on circular orbits with eccentricity errors introduced by observationally allowed inner masses. Furthermore, whilst the inner masses required for  $\eta$  Tel-B and HD 130948-B, -C to be circular in the sky plane are observationally excluded, the maximum allowed inner masses could introduce eccentricity errors of 30% and 20% respectively. We found no upper mass limits in the literature for companions  $\sim 5$  AU from PZ Tel-A, however the  $\sim 200 M_J$  inner mass required to cause a large eccentricity error should be easily detectable. Therefore this scenario may be quickly confirmed or excluded for this system.

In the second case, where the assumed line of sight position and velocity are varied, we see that many of the companions could actually be on circular orbits. However three of the systems must have some astrometric eccentricity regardless of orbital plane. Of these, Gl 229-B and GQ Lupi-B could be on circular orbits with their apparent eccentricity induced by unseen inner masses. Again we have no upper mass limits from the literature for companions close to PZ Tel-A, however the  $130 M_J$  required could well be detectable with current instruments.

It is clear that the inner objects required for this scenario are typically tens of Jupiter masses, and many of them would inhabit the brown dwarf desert which could make their existence unlikely (Marcy & Butler 2000). However it must be noted that brown dwarfs are occasionally observed in these locations (e.g. De Lee et al. 2013), and hence such objects may not be rejected purely due to this consideration.

## 6 DETECTABILITY OF THE UNSEEN MASS

Throughout this paper we have required a massive, unseen inner object to significantly affect the orbital elements of an outer companion. Such large masses may of-

ten be ruled out using observational constraints, however we emphasise that this is by no means the case for all systems. We now summarise several detection methods which may provide upper limits on these masses.

Firstly there are limits from the images themselves. Whilst direct imaging is the best means to detect wide separation companions, it is less suited to objects closer to the star owing to the huge contrast between the stellar flux and that of a smaller mass. The contrast ratio between a Jupiter mass planet and a solar type star is  $10^{-7}$  in the infrared (Traub & Oppenheimer 2010), and that of a brown dwarf to such a star is  $10^{-3}$  to  $10^{-6}$  for L0 to T6 dwarfs respectively (Figure 2.9, Bernat 2012). Whilst such contrast sensitivities are just beginning to be reached at wide angles from stars, companion detectability rapidly worsens closer in. For example the Gemini Deep Planet Survey of young, nearby FGKM stars did achieve contrast sensitivities of  $10^{-7}$  in some cases, but this value degraded sharply within  $4''$  of the stars to around  $10^{-5}$  at  $1''$  (Lafrenière et al. 2007). Similarly the International Deep Planet Survey of A and F stars, which also focussed on young nearby systems, reached contrast ratios of  $10^{-7}$  for some objects but only at separations greater than  $6''$  (Vigan et al. 2012). At the distances of stars with wide separation imaged companions (Figure 11) these angular scales correspond to tens or hundreds of AU, which are much larger than the semi-major axes of masses typically required to introduce a significant error on an outer body's eccentricity.

Projects such as SPHERE (Dohlen et al. 2006), GPI (Macintosh et al. 2006) and Project 1640 (Hinkley et al. 2008) should significantly increase the contrast sensitivity close to the star, and could rule out some of the inner companions required in this paper. However even these instruments would struggle to identify objects of several to tens of Jupiter masses 5–10 AU from stars at 50 pc (Figure 4, Beichman et al. 2010). A further problem lies in actually converting these contrast sensitivities into upper mass limits; this is not a problem in older systems, but is a challenge for objects orbiting young stars. This is because at early ages ( $\lesssim 100$  Myr) hot and cold start models produce significantly different estimates of a companion's luminosity (Spiegel & Burrows 2012). Young companions are also brighter (Marley et al. 2007) and hence more likely to be detected, which means that this problem is commonly encountered. All these considerations mean that for now direct imaging is not the best means to locate or exclude inner objects, although in many cases it provides the only mass constraint in the absence of any other detection method being applied.

The best upper limits on the masses of potential inner companions are likely to come from the radial velocity (RV) technique, which is very good at detecting large objects orbiting close to the star. For a circular inner mass to be undetected to  $3\sigma$  if RV data is available for at least half an orbit,

$$\mu \sin i \lesssim 3 \times 10^{-4} \left( \frac{m_*}{1M_\odot} \right)^{-1/2} \left( \frac{a_i}{10\text{AU}} \right)^{1/2} \frac{K}{1\text{m/s}} \quad (23)$$

where  $i$  is the inclination ( $i = 0$  being face on) and  $K$  is the  $1\sigma$  radial velocity sensitivity.  $K$  is of the order of 1

Companion	Face on orbit				Minimum astrometric eccentricity orbit					
	$e'_{I=0}$	$\tau$	$m_i$ (M <sub>J</sub> )	$a_i$ (AU)	Allowed?	$e'_{\min}$	$\tau$	$m_i$ (M <sub>J</sub> )	$a_i$ (AU)	Allowed?
Gl 229-B	0.9	0.003	47	1.8	Yes	0.3	0.002	15	1.8	Yes
PZ Tel-B	1.0	0.04	210	5.5	-	0.6	0.06	130	5.5	-
$\eta$ Tel-B	1.0	0.006	260	14	No	0.0	0.006	-	-	-
GJ 504-b	0.3	0.004	49	2.6	Yes	0.0	0.004	-	-	-
GQ Lupi-B	0.9	0.002	50	3.7	Yes	0.9	0.002	50	3.7	Yes
GSC 06214-00210-b	0.2	0.0004	5	3.7	Yes	0.0	0.0003	-	-	-
HD 130948-B, -C	1.0	0.03	18	10	No	0.0	0.030	-	-	-

**Table 2.** Locations and masses of the least massive inner objects required to give observed companions certain astrometric eccentricities, if the companions are in fact on circular orbits. The eccentricities in the  $e'_{I=0}$  column have been derived with their orbits confined to the sky plane, and those in the  $e'_{\min}$  column have been calculated by varying the assumed line of sight position and velocity until a minimum  $e'$  was found. The “Allowed?” column states whether this inner mass is observationally permitted. Note that  $\eta$  Tel has a debris disk which lies roughly in the sky plane. We found no upper mass limits in the literature for companions  $\sim 5$  AU from PZ Tel-A.

m/s for current techniques (Pepe et al. 2011). Whilst this method is therefore sensitive enough to rule out many unseen masses of the type described in this paper it is not without its limitations. Most importantly, the detection limit in Equation 23 becomes significantly degraded when the observational baseline is longer than the inner object’s orbital period. Indeed, even if the acceleration from the companion remains at a detectable level, the interpretation of such long-term RV trends remains unknown until one full orbital period has been sampled (e.g. Crepp et al. 2013). In addition the star must be spectrally stable, which means RV is less effective at finding companions in young systems and particularly about A stars (e.g. Galland et al. 2006). Rotational broadening is also a problem for these stars. However it is in these systems that imaging of outer companions is most successful, due to the decreasing companion luminosity with time (Baraffe et al. 2003). For this reason RV and imaging surveys do not usually target the same stars, although there is some overlap between the two techniques. Finally RV cannot detect companions if the system is face on, which is the orientation favoured if the outer companion’s motion is to be determined via direct imaging. As a result of these caveats many stars, including almost all of the systems on Figure 11, do not have RV data so large inner masses may not be ruled out. Indeed the detection of an eccentric outer companion could provide motivation for RV follow-up, to investigate whether an unseen inner mass is also present and responsible for this apparent high eccentricity.

Finally, stellar astrometry is also reaching the sensitivities required to detect companions, and this method is most sensitive to face-on orbits so could detect those missed by RV. However this method also requires a baseline longer than the inner mass period. If such precision astrometry is available, the object may remain undetected to  $3\sigma$  if

$$\mu \lesssim 2 \times 10^{-2} \left( \frac{a_i}{10\text{AU}} \right)^{-1} \frac{d}{50\text{pc}} \frac{\theta_{\text{ast}}}{1\text{mas}} \quad (24)$$

where  $\theta_{\text{ast}}$  is the astrometric accuracy, which is currently of the order 1 mas if many reference stars are available in the same field (e.g. Benedict et al. 2002; Sozzetti 2005).

Due to the required baseline, it is still possible for Jupiter - brown dwarf mass objects to exist at  $\gtrsim 10$  AU and remain undetected by precision astrometry.

The upcoming GAIA mission will bring about a significant improvement in astrometric precision, promising to reach sensitivities of  $8 \mu\text{as}$  (Casertano et al. 2008). However even GAIA will not be able to rule out many massive inner companions, due to the requirement it observes the star for at least one full orbit of the inner body. Using the detection limits from Figures 21 and 22 in Casertano et al. (2008) we see that whilst Jupiter mass planets could be detected to three sigma at 2-3 AU from solar type stars out to 200 pc, objects with significantly larger masses could still lie further out as the companion period increases beyond the 5 yr lifetime of the mission. In fact, brown dwarf mass objects could still exist undetected down to 10–20 AU from  $1M_{\odot}$  stars at 10 pc, which means that GAIA will not be able to rule out many of the inner objects required for the scenario in this paper.

## 7 DISCUSSION

We have shown that the orbital elements of an imaged companion may be incorrectly derived due to the presence of an unseen inner mass. We demonstrated that a circular object would always appear eccentric if an inner mass were introduced, and showed that a non-negligible time between observations reduces the effect of this unseen mass on the companion’s orbital elements. We then provided a framework to identify the maximum eccentricity error an unseen mass could introduce as a function of readily derivable parameters, and also found the optimum location of such an object. We demonstrated that many imaged companions could potentially be susceptible to this error, and showed that the eccentricity of Fomalhaut-b could be have been overestimated by up to 10%. Finally we showed that the large inner masses required by this scenario are not always ruled out by other observations. We will now remark on a few other considerations about this work.

Firstly, we have only examined the effect of an inner mass on the elements of an object that is known to be bound. Another potential application of this scenario

is on the initial identification of the companions themselves. If an inner mass lay undetected in a system with a highly eccentric imaged outer object, the stellar velocity shift due to this unseen mass could increase the apparent eccentricity of the observed companion beyond unity. In other words, this effect could actually make a bound companion appear unbound. It is unlikely that such a companion would be classified as a background object, as this would require its apparent motion to mimic that expected of a background source. However one could envisage a scenario where this effect could be important, for example if searching for companions around young stars still in stellar associations. Here an unseen inner mass could lead to a bound imaged object being misidentified as an unassociated member of the same moving group.

As an example we examined the survey of Janson et al. (2011), who imaged 18 massive stars in the solar neighbourhood to search for potential companions. We find three stars amongst their sample, Bellatrix (HIP 25336), Elnath (HIP 25428) and  $\lambda$  Aquilae (HIP 93805), which each have point sources located nearby with apparent relative velocities only just large enough to make them unbound. We find that, were unseen inner masses of 50-100  $M_J$  located close to these stars (which are below the detection limits for this survey at the required radii), the point sources could be bound (albeit with a high eccentricity). Such sources would be unlikely to be re-imaged in the near future as no companions were identified, so it could be that bound objects are missed. Whilst we consider this unlikely for these three stars due to the large inner masses required, it does highlight the potential importance of this effect for survey work.

Secondly we have only considered two epochs of observation in this paper, which is the minimum number required to estimate the outer body's orbital elements. If more epochs were available, the method presented here would still be applicable so long as the motion of the outer companion appeared linear over the entire observational baseline. In this case the companion positions could be fitted with a linear trend and the problem treated as before. If instead the additional epochs allowed orbital acceleration to be detected then  $\tau$  would be too large for an inner body to significantly affect the companion's elements anyway, and so the scenario in this paper would not be applicable.

There is one difference between the use of two and three or more observations however. If an inner object existed with a period less than the time between the first and last observations, the motion of the outer companion should not in fact be linear but should show short term oscillations as the inner binary rotates. This could potentially be identified using the additional observations between the first and last epochs. If such oscillatory motion were detected then this would provide strong evidence for the presence of an unseen companion, and its orbital properties could be constrained. Alternatively if no such motion were observed then it may be possible to rule out significant unseen masses with periods shorter than the observational baseline.

Finally we have assumed that the inner mass is on a circular orbit throughout this work, as this requires fewer parameters than a more general case where both bodies

are eccentric. However this need not be the case. As the difference between the astro- and barycentric coordinates of the outer companion increases with the velocity of the star in the barycentric frame, it is clear that this difference may be increased if the inner mass were eccentric and at pericentre when the system was observed. Indeed, the optimum set-up for this scenario would be if both the inner and outer bodies had their orbits aligned (i.e. pericentres in the same direction), and both were near pericentre at the time of the observations. However this exact set-up is unlikely, due to the precise alignment involved. To test this we generated  $10^7$  systems with randomised parameters, each consisting of a wide eccentric companion and a coplanar inner mass. Half of the systems had eccentric inner masses, whilst the other half had them on circular orbits. For each system we randomised the mean anomalies of these two bodies and calculated the astrometric elements of the outer companion. We find that making the inner mass eccentric almost always leads to a lower eccentricity error for the outer body, because it is much rarer for the star to have a velocity shift that exactly opposes the outer companion's motion. Also the optimum case, where both bodies are at pericentre at the time of the observation, is very rare because the bodies do not spend much time around pericentre. The odds of making an observation in this configuration are therefore very low. Hence we conclude that, whilst the eccentricity error on an observed companion may be increased if the inner body is eccentric, in practise the error is almost always reduced in this regime. We have therefore not considered this any further.

## 8 CONCLUSIONS

We have shown that the use of direct imaging to derive the orbital elements of companion planets/brown dwarfs could lead to significant errors if an undetected inner mass is also present. The maximum effect of such a body on the derived eccentricity (and hence semi-major axis) of the observed companion has been quantified for various cases, and we have also identified criteria to determine when this effect may be significant. We provide the reader with a step-by-step method to determine the maximum magnitude of this effect for any system, and apply it to several companions as examples. It appears that many of the currently imaged companions could be susceptible to this scenario when they have orbital motion detected.

## REFERENCES

- Baraffe I. et al., 2003, *A&A*, 402, 701
- Beichman C. A. et al., 2010, *PASP*, 122, 162
- Benedict G. F. et al., 2002, *ApJ*, 581, L115
- Bernat D., 2012, PhD thesis, Cornell Univ.
- Boss A. P., 2011, *ApJ*, 731, 74
- Casertano S. et al., 2008, *A&A*, 482, 699
- Chauvin G. et al., 2004, *A&A*, 425, L29
- Chauvin G. et al., 2005, *A&A*, 430, 1027
- Chauvin G. et al., 2012, *A&A*, 542, A41



- Crepp J. R. et al., 2012, *ApJ*, 751, 97  
 Crepp J. R. et al., 2013, *ApJ*, 771, 46  
 De Lee N. et al., 2013, *AJ*, 145, 155  
 Delorme P. et al., 2013, *A&A*, 553, L5  
 Dohlen K. et al., 2006, *Proc. SPIE*, 6269, 62690Q  
 Exoplanet.eu, 2013, accessed 24 May 2013, <exo-planet.eu>  
 Galland F., 2006, *A&A*, 447, 355  
 Gaudi B. S., 2012, *ARAA*, 50, 411  
 Ginski C. et al., 2013, 434, 671  
 Gladman B., 1993, *Icarus*, 106, 247  
 Golimowski D. A. et al., 1998, *AJ*, 115, 2579  
 Hinkley S. et al., 2008, *Proc. SPIE*, 7015, 701519  
 Ireland M. J. et al., 2011, 726, 113  
 Janson M. et al., 2011, *ApJ*, 736, 89  
 Kalas P., Graham J. R. & Clampin M., 2005, *Nat*, 435, 1067  
 Kalas P. et al., 2013, *ApJ*, 775, 56  
 Kasper M. et al., 2007, *A&A*, 471, 655  
 Kennedy G. M. et al., 2013, *MNRAS*, in press  
 Kenworthy M. A. et al., 2009, *ApJ*, 697, 1928  
 Kenworthy M. A. et al., 2013, *ApJ*, 764, 7  
 Krist J., 2006, in *Coronagraph Workshop 2006*, Traub W. A., ed., NASA, p. 83  
 Kuzuhara M. et al., 2013, 774, 11  
 Lafrenière D. et al., 2007, *ApJ*, 670, 1367  
 Lagrange A. -M. et al., 2009, *A&A*, 493, L21  
 Lagrange A. -M. et al., 2012, *A&A*, 542, L18  
 Le Bouquin J. -B. et al., 2009, *A&A*, 498, L41  
 Lee M. H. & Peale S. J., 2003, *ApJ*, 592, 1201  
 Lin D. N. C. & Ida S., 1997, *ApJ*, 477, 781  
 Lissauer J., 1993, *ARAA*, 31, 129  
 Macintosh B. et al., 2006, *Proc. SPIE*, 6272, 62720L  
 Malmberg D., Davies M. B. & Hoggie D. C., 2011, *MNRAS*, 411, 859  
 Marcy G. W. & Butler R. P., 2000, *PASP*, 112, 137  
 Marley M. S. et al., 2007, *ApJ*, 655, 541  
 Marois C. et al., 2008, *Sci*, 322, 1348  
 Marois C. et al., 2010, *Nat*, 468, 1080  
 Marzari F. & Weidenschilling S. J., 2002, *Icarus*, 156, 570  
 Metchev S. A. & Hillenbrand L. A., 2004, *ApJ*, 617, 1330  
 Metchev S. A. & Hillenbrand L. A., 2006, *ApJ*, 651, 1166  
 Morbidelli A., 2002, *Modern Celestial Mechanics: Aspects of Solar System Dynamics*. Taylor & Francis, London, p. 16  
 Mugrauer M. et al., 2012, *MNRAS*, 424, 1714  
 Nakajima T. et al., 1995, *Nat*, 378, 463  
 Neuhäuser R. et al., 2008, *A&A*, 484, 281  
 Neuhäuser R. et al., 2010, *A&A*, 516, A112  
 Neuhäuser R. et al., 2011, *MNRAS*, 416, 1430  
 Pepe F. et al., 2011, *A&A*, 534, A58  
 Reid I. N. et al., 2001, *ApJ*, 121, 489  
 Rodrigues T. J. & Hinz P. M., 2009, *ApJ*, 702, 716  
 Rodriguez D. R. et al., 2012, *ApJ*, 748, 30  
 Ségransan D. et al., 2011, *A&A*, 535, A54  
 Smith R. et al. 2009, *A&A*, 493, 299  
 Soummer R. et al., 2011, *ApJ*, 741, 55  
 Sozzetti A., 2005, *PASP*, 117, 1021  
 Spiegel D. S. & Burrows A., 2012, *ApJ*, 745, 174  
 Tanner A. M., Gelino C. R., & Law N. M., 2010, *PASP*, 122, 1195  
 Traub W. A. & Oppenheimer B. R., 2010 in *Exoplanets*, Seager S., ed., 2010, Univ. Arizona Press, Tucson, p. 111  
 Vigan A. et al., 2012, *A&A*, 544, A9  
 Watson C. A. et al., 2011, *MNRAS*, 413, L71  
 Wilson J. C. et al., 2001, *ApJ*, 122, 1989  
 Wittenmyer R. A. et al. 2013, *ApJS*, 208, 2  
 Zuckerman B. & Song I., 2009, *A&A*, 493, 1149

## APPENDIX A: MIN( $\mu$ ) EQUATION FOR THE $E \neq 0$ CASE

Here we present a simplified equation for the minimum value of  $\mu$  required to give an eccentric outer object an astrocentric eccentricity  $e'$  if the time between observations is small. This is analogous to the  $e = 0$  case given by Equation 5, and shows good agreement with the lines on Figure 8. As for the simpler case the full version of this expression contains high orders of  $\mu$ , however terms arising from orders greater than two are now less dominant because the equation now includes a first order term inside the square root. Therefore the following formulae (up to second order in  $\mu$ ) are sufficiently accurate without an empirical scaling factor:

$$A\mu^2 + B\mu + C \gtrsim 0, \quad (\text{A1})$$

where

$$\begin{aligned}
 A \equiv & \alpha^2 \frac{(1+e)(3+e)}{(1-e)^2} \\
 & + (2e+1) \left( 2\alpha \frac{1+e}{1-e} + 4\sqrt{\alpha} \sqrt{\frac{1+e}{1-e}} + \frac{4}{\sqrt{\alpha}} \sqrt{1-e^2} \right) \\
 & + \frac{2}{\alpha} (2+3e)(1-e) + (1+e)^2,
 \end{aligned}$$

$$B \equiv 2e \left( 1+e + \alpha \frac{1+e}{1-e} + \frac{2}{\sqrt{\alpha}} \sqrt{1-e^2} \right),$$

$$C \equiv e^2 - e'^2,$$

which may be solved for  $\mu$ . Note that as  $e \rightarrow 0$ ,  $B \rightarrow 0$  and the solution tends to that of Equation 5, and so in this case the empirical factor  $F(e')$  will again be required.